EVAPOTRANSPIRATION AND LAND SURFACE PROCESS RESPONSES TO AFFORESTATION IN WESTERN TAIWAN: A COMPARISON BETWEEN DRY AND WET WEATHER CONDITIONS

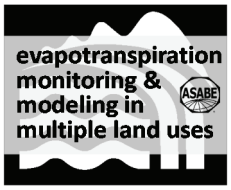

Y.-Q. Liu, L. B. Zhang, L. Hao, G. Sun, S.-C. Liu

ABSTRACT. *An afforestation project was initiated in the western plain of Taiwan to convert abandoned farming lands into forests to improve the ecological and environmental conditions. This study was conducted to understand the potential impacts of this land cover change on evapotranspiration (ET) and other land surface processes and the differences in the impacts under clear and rainy weather conditions. Numerical simulations with the land surface covered with crops and forests were conducted using an atmosphere-land coupled model during a summer monsoon season. Sensitivity experiments were conducted to understand the possible impacts of the convection and atmospheric planetary boundary layer parameterization schemes used in this study on the simulation results. The results of the entire simulation period indicate that, although the maximum solar radiation is increased by 30 W m^{-2} from about 800 W m^{-2} due to smaller albedo after afforestation, the maximum ET near noon time is decreased by about 3 mm h^{-1} from about 17 mm h^{-1} on clear days, mainly due to increased stem area index and reduced wind speed within the forest canopies. Meanwhile, the maximum sensible heat flux is increased by about 100 W m^{-2} from 200 W m^{-2} due to larger total vegetation area (the sum of leaf and stem area index) in forests. Similar responses in ET and other land surface processes to the afforestation are obtained for clear weather conditions. In contrast, ET is increased and sensible heat flux is decreased under rainy conditions. The changes in ET are more important on clear days than on rainy days in determining the responses over the entire simulation period. The sensitivity experiments confirmed the simulated responses of ET and other land surface processes. The results suggest that afforestation would modulate hydrological cycles by reducing ET on clear days and elevating ET on rainy days, thereby reducing the risks of hydrological extremes.*

Keywords. *Afforestation, Dry and wet conditions, Evapotranspiration, Regional climate modeling, Taiwan.*

Land use and land cover types have changed from time to time in many regions of the world (Sampson, 2004) due to human activities and climate change. Massive deforestation has occurred worldwide, converting forests to farming lands, urban, and other land uses. Subtropical and temperate North America, Europe, and Asia during the late 19th century and early 20th century and tropical South America and Africa during the middle and late 20th century have seen most of the deforestation to meet the needs for rapid economic development and population growth. For example, forest acreage in the U.S. declined in the 19th century and early 20th century, reaching the lowest level around the 1920s as a result of agricultural land clearing and timber harvesting (USDA Forest Service, 1994).

This deforestation trend reversed later in some regions, mainly to address ecological and environmental concerns. In the U.S., the Civilian Conservation Corps program was initiated during the Great Depression. About 3 billion trees were planted from 1933 to 1942 that turned a large portion of agricultural and abandoned logging lands into forests in the U.S. Southeast and Midwest. In China, the Three-North Shelter Forest Program (the Green Great Wall) started in the late 1970s (Fang et al., 2001; Zhang et al., 2007; Liu et al., 2008b) aiming to increase forest cover from 5% to 15% in northern China by 2050 when the project is completed. Today, China has the most planted forests in the world (>0.5 million km^2), contributing to the recent dramatic increase of national forest coverage to 18%. In Africa, about 20 countries agreed upon the Sahel Initiative to build a

Submitted for review in December 2014 as manuscript number NRES 11110; approved for publication by the Natural Resources & Environmental Systems Community of ASABE in October 2015.

Mention of company or trade names is for description only and does not imply endorsement by the USDA. The USDA is an equal opportunity provider and employer.

The authors are **Yongqiang Liu,** Research Meteorologist, Center for Forest Disturbance Science, USDA Forest Service, Athens, Georgia; **Libo Zhang,** Graduate Student, and **Lu Hao,** Professor, International Center for Ecology, Meteorology, and Environment (IceMe) and Jiangsu Key Laboratory of Agricultural Meteorology, Nanjing University of Information Science and Technology, Nanjing, China; **Ge Sun,** Research Hydrologist, Eastern Forest Environmental Threat Assessment Center, USDA Forest Service, Raleigh, North Carolina; **Shaw Cheng Liu,** Professor, Research Center for Environmental Changes, Academia Sinica, Taipei, Taiwan. **Corresponding author:** Yongqiang Liu, Center for Forest Disturbance Science, 320 Green St., Athens, GA 30602; phone: 706-559-4240; e-mail: yliu@fs.fed.us.

"Great Green Wall" by planting trees on the southern edge of the Sahara desert to slow desertification (Schleeter, 2013).

Forest deforestation or afforestation can affect evapotranspiration (ET) and other hydrologic processes through changing vegetation properties such as albedo, leaf area index (LAI), and surface roughness (Pielke et al., 2011; Jones et al., 2012; Sun and Liu, 2013). When land cover is replaced with a different type of vegetation, surface albedo is changed, leading to different solar radiation absorbed on the ground, directly affecting heat energy available for evapotranspiration. LAI is an important land surface characteristic that controls seasonal evapotranspiration dynamics. Forests have a larger LAI than bared land or short crops and therefore can generally intercept more precipitation and transfer more water from soils to the atmosphere through transpiration. Forest canopies usually have larger roughness and therefore intensify water and heat transfer with the atmosphere through reducing aerodynamic resistance. Because energy and water balances are tightly coupled, the changes in energy balances can impact local and regional hydrology (Jackson et al., 2005; McVicar et al., 2007).

Large-scale land cover change also occurred in the western plain of Taiwan. This region was originally covered by primary forests that are commonly found on the other side of the mountain ranges today. Cultivation and settlement centers were established mostly in the 18th century when immigrants from mainland China moved to Taiwan (Liu, 1998). With the rapid population growth and industrial development in the middle 20th century, many farm lands were replaced by urban construction. Similar to other regions in the world, the land cover changes have resulted in many hydrological and environmental consequences (Wu et al., 2001; Lin et al., 2008). For example, Wu et al. (2001) found significant increase in runoff and decrease in groundwater recharge when a rice paddy field was converted to a dry farming field. Since globalization of the economy started in the early 2000s, farming has become less or even no longer profitable for farmers in Taiwan. As a result, some farming lands have been abandoned and have caused ecological and environmental problems. A regional "Afforestation in the Flat Area" project to reforest the abandoned lands was initiated to improve the living environment and resources as well as to mitigate the impacts of global warming (Shen, 2009).

When compared to bared or less vegetated land surfaces, ET rates of trees or forests are higher in general, and thus streamflow is lower in forest-dominated watersheds. Worldwide "paired watershed" experiments have confirmed this general conclusion: afforestation increases ET and decreases streamflow (Sun and Liu, 2013). However, the impacts of afforestation on local and regional climate and hydrology vary substantially with latitude, topography, and size of afforestation. For the thermal effects, for example, Li et al. (2015) indicated that afforestation generally leads to a strong cooling effect throughout the year in tropical regions, moderate cooling in summer but moderate warming in winter with net cooling annually in temperate regions, and strong warming in winter and moderate cooling in summer with net warming annually in boreal regions. Taiwan is an island located in the transition zone of tropical and subtropical climate regimes with complex topography of the western flat plain and the eastern mountain ranges. The possible differences in the impacts of afforestation on climate and hydrology between this region and other tropical regions are not clear.

The purpose of this study was to understand and quantify the potential hydrological responses to afforestation in the western plain of Taiwan. Hourly and daily ET and other land surface processes were examined through numerical simulations with the National Center for Atmospheric Research (NCAR) regional climate model (RCM) RegCM (Giorgi et al., 1993a, 1993b) with 10 km resolution for June 1994.

METHODS

REGION

The Taiwan island, with an area of about 36,000 km^2, is located about 200 km southeast of the coast of mainland China across the Taiwan Strait. The topography of the island is characterized by the contrast between the western flat plain and the eastern mountain ranges, which peak at nearly 4000 m. The land use types are mainly agriculture and urban in the west and forests in the east. Figure 1 shows the land types of the simulation domain. About one-fourth of the land (9,000 km^2) is under cultivation, mainly rice paddy along the western plain and in the south. As described below, the Biosphere-Atmosphere Transfer Scheme (BATS) (Dickinson et al., 1993) was used to simulate the land surface processes. The BATS scheme has 18 land types, but urban is not included and therefore no urban areas are shown in figure 1. The annual rainfall is around 2500 mm, and the summer temperature is around 28°C. The climate is influenced by the East Asian monsoon, with summer monsoon (from May to October) rainfall accounting for 90% of the annual rainfall in the south and 60% in the north.

CLIMATE MODEL

RegCM was used for this simulation study. RegCM is a

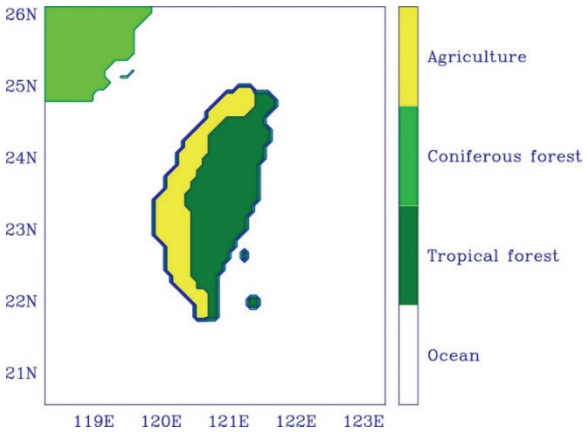

Figure 1. Land cover types of Taiwan and the surrounding areas.

numerical tool for simulating physical conditions and changes in the atmosphere coupled with vegetation and the soil. It was developed in the late 1980s at NCAR (Dickinson et al., 1989; Giorgi and Bates, 1989) based on the standard Penn State/NCAR Mesoscale Model Version 4 (MM4) (Anthes et al., 1987) through including more detailed descriptions of some physical processes important to climate, including radiation, land surface, planetary boundary layer (PBL), and precipitation. These processes are very simple or not included in a weather model because they may not be important for short-term atmospheric variations. RegCM was used and evaluated in regional climate modeling of East Asia (Liu et al., 1994, 1996).

RCMs address some of the scale issues associated with low-resolution global general circulation models (GCMs) in modeling regional climate. GCMs mostly have spatial resolutions of several hundred kilometers, and the effects of local and regional forcing such as terrain and land cover variability are often not well represented. RCMs, on the other hand, have spatial resolutions of tens of kilometers or higher, are often equipped with more detailed schemes for local and regional properties, and are therefore a better tool for understanding climate at regional scale. However, unlike GCMs, which can be run for as long as thousands of years, RCMs usually are run from months to years because of the extreme computer time consumption due to the higher resolution and more detailed description of physical processes.

SIMULATIONS

The simulation domain covered the Taiwan island and the surrounding areas, centered at 23.5° N and 121° E. The domain had 60 × 70 grid points, a horizontal resolution of 10 km, and 14 vertical layers up to 80 hPa. The simulation was conducted for June 1994. As indicated by Misra and Dirmeyer (2009), the hydroclimate in summer is generally more active, with equally active convective precipitation that serves as a conduit between the surface fluxes and precipitation. In addition, based on the Clausius-Clapeyron relation, the absolute humidity in the atmospheric column is larger in summer than in winter, This raises the moist static energy, which gives rise to relatively stronger convective activity and potentially larger influence of boundary forcing differences on the water cycle.

The initial and horizontal lateral boundary conditions of wind, temperature, water vapor, and surface pressure were interpolated from the analysis of the European Center for Medium Range Weather Forecast (ECMWF) with a resolution of 1.875° (Trenberth and Olson, 1988). Soil water content initialization was described by Giorgi and Bates (1989) based on the specified vegetation type. Time-dependent sea surface temperature was interpolated from a set of observed monthly means with a resolution of 0.5° (Shea et al., 1992). The precipitation and temperature data used for simulation evaluation were obtained from weather stations in Taiwan (available at tutiempo.net/en/Climate/Taiwan/TW.html).

Water and heat fluxes on the land surface were calculated through BATS. BATS includes a set of equations for soil and vegetation energy and water balances to predict temporal variations of temperature and moisture, parameterizations schemes to estimate fluxes of heat and water, and specifications of physical parameter values. All parameters are provided for 18 types of land cover and 12 classes of soil texture. The vegetation within a grid cell is assumed to be a "big leaf" instead of individual trees. BATS has three soil layers (the surface, root zone, and a third layer between the root zone and the groundwater) extending from the soil surface to 0.1 m, 1 or 2 m (depending upon land cover type), and 3 m, respectively. Soil moisture of each layer is modeled as a function of precipitation, evapotranspiration, and runoff. Soil moisture is also affected by soil-vegetation water exchanges through root water uptake in the root zone and water exchange with the groundwater in the third layer. Runoff is proportional to soil moisture and water balance between precipitation and evapotranspiration. The water level of the groundwater layer is assumed to be constant, despite the finding that the water level could fluctuate remarkably during a prolonged drought event. There are no horizontal interactions between grid cells. The BATS scheme was integrated at a time step of 3 min. Water and heat fluxes were calculated for the entire grid cell (10 km).

In addition to evaporation from the bared ground surface, soil water is transported through transpiration to the foliage surface and then evaporated into the surrounding air. The evaporation (E_f) and sensible heat flux (H_f) from the foliage surface are calculated as:

$$E_f = \rho_a [r_a^{-1} L_w + (r_a + r_s)^{-1} L_d](q_f^{sat} - q_{af}) \quad q_f^{sat} \geq q_{af} \tag{1}$$

where
ρ_a = air density
r_a = aerodynamic resistance
L_w = fractional water on leaves, which is determined by precipitation intercepted by leaves
r_s = stomatal resistance
$L_d = (1 - L_w)(\mathrm{LAI}/L_{\mathrm{SAI}})$
q_f^{sat} and q_{af} = corresponding saturation humidity of foliage surface and specific humidity of air inside canopy.

$$H_f = C_p \sigma_f L_{\mathrm{SAI}} r_a^{-1} (T_f - T_{af}) \tag{2}$$

where
C_p = heat capacity
σ_f = fractional vegetation cover
L_{SAI} = sum of LAI and stem area index (SAI)
T_f and T_{af} = temperatures of foliage surface and air inside the canopy, respectively.

$$r_a^{-1} = C_f \left(\frac{V_a k}{C_R \ln(z_1 / z_0)^2 D_f} \right)^{1/2} \tag{3}$$

where
C_f = constant
V_a = wind speed above the canopy

k = von Karman constant
C_R = a parameter depending on surface bulk Richardson number, which is a function of vertical temperature gradient
z_0 and z_1 = roughness length and height of the lowest atmospheric level
D_f = characteristic dimension of leaves in the direction of wind flow.

$$r_s = r_{\min} R_l S_l M_l \quad (4)$$

where
$r_{\min}$ = minimum value of stomatal resistance
R_l, S_l, and M_l = net radiation, temperature, and soil moisture factors for stomatal resistance.

The key BATS parameters used for this study are presented in table 1. Different albedo values are assigned to visual (wavelength <0.7 μm) and near-infrared (wavelength ≥0.7 μm) solar radiation. Soil albedo is a sum of a value for saturated soil and a factor that increases with soil dryness. The albedo for saturated soil depends on soil color and is about 0.85 (wavelength <0.7 μm) and 0.17 (wavelength ≥0.7 μm) averaged over all eight soil colors in BATS. No soil type and color changes were made in this study. LAI is a sum of its minimum value and the difference between maximum and minimum values with a temperature factor. LAI reaches its largest value in summer and smallest value in winter. The LAI values in BATS vary with season remarkably for crops but little for rainforests. The maximum values are the same and were used for this study. SAI is a constant for each land cover type. Fractional foliage cover varies with season for both crop and forest. It has the largest values during summer of 0.85 for crop and 0.9 for forest, which were used for this study. Roughness, an indicator of plant height, is a constant value for each land cover type in BATS.

The Kuo scheme (Kuo, 1974; Anthes, 1977) was used to simulate convective precipitation. This scheme assumes that convections occur when the atmosphere becomes unstable with moisture convergence. Some converged moisture increases atmospheric humidity, and some is converted into rainfall. The core of this scheme is to determine the partition based on water and energy balances. The Kuo scheme is simple but less capable of reproducing realistic convection.

The nonlocal scheme developed by Holtslag et al. (1990, 1993) was used to describe the PBL processes. In addition to the traditional vertical gradient of average air properties, the scheme also includes counter-gradient fluxes resulting from large-scale eddies in an unstable, well-mixed atmosphere when calculating turbulent diffusion. The counter-gradient fluxes are determined by the surface temperature or water vapor flux, the turbulent convective velocity that depends on the friction velocity, and the PBL height.

Table 1. Parameters for crop and forest in BATS.

Parameter	Crop	Forest
Albedo (wavelength <0.7 μm)	0.1	0.04
Albedo (wavelength ≥0.7 μm)	0.3	0.2
Maximum LAI	6.0	6.0
Stem area index (SAI)	0.5	2.0
Maximum fractional foliage	0.85	0.9
Roughness (m)	0.06	2.0

RegCM uses the NCAR Community Climate Model (CCM) radiative transfer package (Briegleb, 1992; Kiehl et al., 1996). The solar component accounts for the radiative effects of O_3, H_2O, CO_2, and O_2. It includes 18 spectral intervals from 0.2 to 5 μm. The cloud scattering and absorption parameterization follows that of Slingo (1989) whereby the optical properties of the cloud droplets (extinction optical depth, single scattering albedo, and asymmetry parameter) are expressed in terms of the cloud liquid water content and an effective droplet radius (Elguindi et al., 2007).

Two simulations were conducted. In the control simulation, the current land use is dominated by rice paddy in the western plain without considering urbanization. In the afforestation simulation, all crop lands are converted into forests at the grid points in the western plain with elevations lower than 500 m. The hydrological impacts of the afforestation are measured by the differences in ET as well as other related fluxes and variables between the afforestation and control simulations. The land types in the simulation domain were specified based on the global 1 km resolution International Geosphere Biosphere Program (IGBP) land cover dataset (Zeng et al., 2000).

SENSITIVITY EXPERIMENTS

There are some limitations with the RegCM modeling technique. RegCM is driven by GCMs and/or meteorological measurements; any errors in lateral conditions will be passed to RegCM. Even though the complex local land surface condition was one of the reasons for using RegCM, information deficiencies limit the ability of RegCM to reproduce important features in the atmosphere and other earth components. Domain size and internal variability created by disturbances in initial and boundary conditions affect RegCM performance (Seth and Giorgi, 1998; Giorgi and Shields, 1999). The RegCM version used for this study is a hydrostatic model, meaning that the vertical pressure gradient force is equal to gravity. This assumption works well for flat land surfaces but causes problems in areas with complex topography, especially for simulations of local convections and circulations (Kato et al., 1999). This would affect simulations in Taiwan, although likely less remarkably for the afforested flat western plain.

RegCM performance could vary substantially depending on the parameterizations of important physical processes of land surface, convection, PBL, radiation, etc. Sensitivity experiments were conducted to understand how robust the simulations results are with varied physical parameterization schemes. The alternative Grell convective scheme (Grell, 1993), developed based on the Arakawa-Schubert scheme (Arakawa and Schubert, 1974), was used. Convective instability in the scheme is produced by large-scale atmospheric processes, while dissipated by small-scale processes. Clouds are represented by an updraft and a downdraft. Condensation within the updraft occurs as a saturated air parcel is lifted. There is only a single dominant cloud type instead of a spectrum of cloud types. In

comparison with the Kuo scheme, the Grell scheme includes more physical processes but is complex and needs longer calculation time. Furthermore, a PBL scheme without including the counter-gradient fluxes was examined. As in the simulations described above (denoted the reference simulations), each sensitivity experiment included control and afforestation simulations, which were conducted over a dry period (June 26-30, 1994) and a wet period (June 1-5, 1994).

Results

Evaluation of Simulated Precipitation and Air Temperature

The simulated mean precipitation and temperature over the western plain were evaluated against daily observations from 22 stations. The distance between two adjacent stations varies but is about 20 km on average. Two major rainfall events with daily rainfall of about 35 mm and 15 mm occurred on June 1 and 18, respectively, in the western plain of Taiwan (fig. 2). A weak rainfall event with daily rainfall around 3 mm occurred during June 5-7. RegCM was able to catch the three precipitation events despite the differences with the observed events in both magnitude and timing. The simulated precipitation is smaller in magnitude by half for the first major event but much larger for the weak event, and the simulated precipitation lasts one day longer for the second major event and starts one day earlier for the weak event. The model had large bias in simulating the first major event and the weak event during the first seven days. The circulation systems that produced both rainfall events during this period and the second major event on June 18 were easterly waves. The airflows moved westward over the ocean east of Taiwan, turned north first and then south over the island, and returned to westward over the ocean west of Taiwan (not shown). The trough line oriented from south to north was over the western plain. The model may have had low capacity in simulating the airflows due to the limitation of the hydrostatic assumption. In contrast, the trough line of the easterly waves for the second major event was located farther west, with the airflows behind the trough line generally over the western plain. The impact of the hydrostatic assumption was relatively smaller.

The observed surface air temperature showed an increasing trend over the simulation period. The values corresponding to the two major rainfall events were relatively low, at about 23.5°C and 26°C, respectively, but rose rapidly following each major precipitation event. The simulated temperature closely follows the observed daily variation. The difference in magnitude is within 1°C in the first 20 days but nearly double that thereafter. The differences are within the acceptable bias range.

Evapotranspiration

The daily ET rates from the control run averaged over the simulation period decrease from about 6 mm d^{-1} in the flat coastal area to 4 mm d^{-1} in the elevated mountains (fig. 3). This spatial pattern is similar to that on a clear summer day in 2002 detected by the MODIS satellite (Zhan et al., 2011). However, the MODIS detection showed a different pattern on a clear summer day in 2003, indicating that ET in summer could be influenced by factors other than topography and land cover type.

The afforestation leads to a decrease in ET by more than 1 mm d^{-1}, a relative change of nearly 20%. The change occurs only in the afforested area. Both ET and its change occur mainly during daytime (fig. 4a). The ET value is very small before 7:00 a.m., gradually reaches a peak around noon, and then decreases until about 7:00 p.m. The change in ET follows a similar diurnal cycle, except with negative values.

Energy Balance

Net radiation, sensible heat, and latent heat are approximately in balance over a long period during which temperature change is relatively small. The simulated net solar radiation on the land surface (vegetation and soil) increases

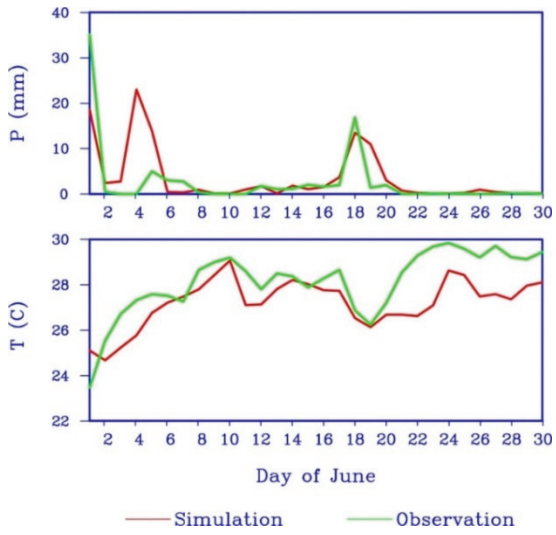

Figure 2. Daily variations of simulated (red) and observed (green) precipitation P (top) and surface air temperature T (bottom) averaged over the western plain of Taiwan.

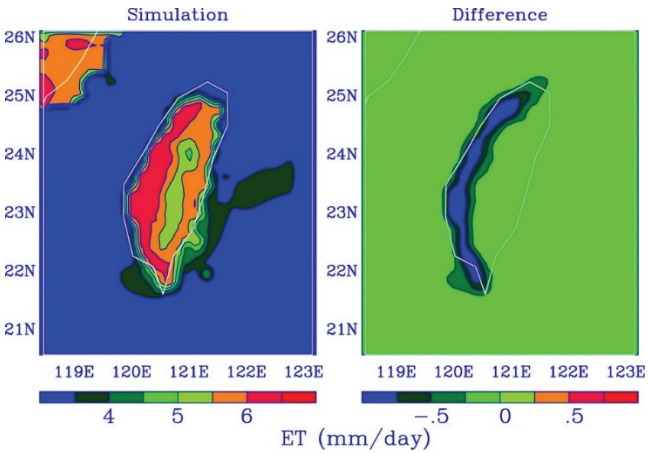

Figure 3. Spatial patterns of ET (mm d^{-1}) averaged over the simulation period for the control simulation (left) and the difference between the afforestation and control simulations (right).

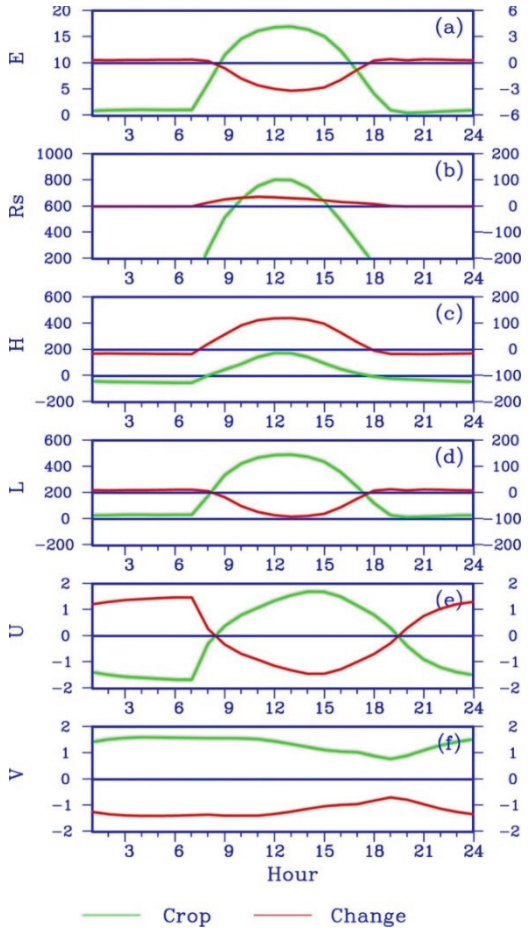

Figure 4. Diurnal cycles of ET from the control simulation (green line, left axis) and the difference between the afforestation and control simulations (red line, right axis) averaged over the simulation period. Panels (a) to (f) are ET (mm h^{-1}), net solar radiation (R_s, W m^{-2}), sensible heat (H, W m^{-2}), latent heat (L, W m^{-2}), zonal wind (U, m s^{-1}), and meridional wind (V, m s^{-1}).

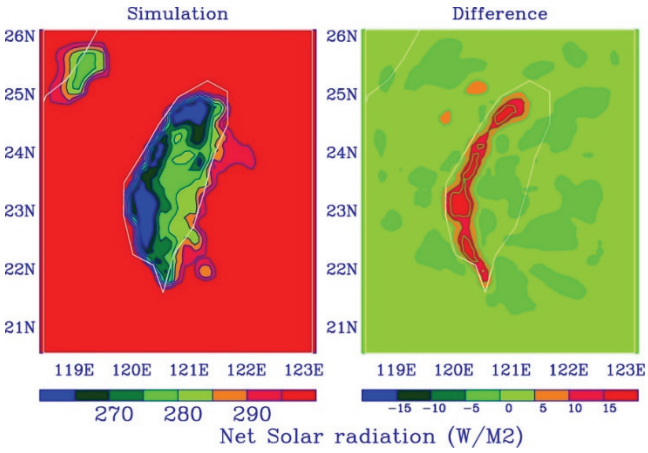

Figure 5. Spatial patterns of daily net radiation (W m^{-2}) averaged over the simulation period for the control simulation (left) and the difference between the afforestation and control simulations (right).

from about 250 W m^{-2} in the western plain to 280 W m^{-2} in the mountain region (fig. 5). Afforestation leads to an increase of up to 20 W m^{-2} during daytime (fig. 4b). Little change occurs in longwave radiation. The increased net solar radiation is simply due to reduced albedo from 0.1

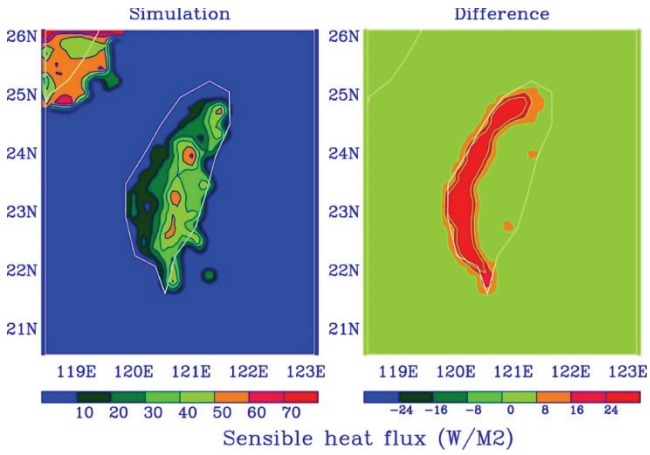

Figure 6. Spatial patterns of daily sensible heat flux (W m^{-2}) averaged over the simulation period for the control simulation (left) and the difference between the afforestation and control simulations (right).

(0.3) with crop to 0.04 (0.2) with forest for wavelengths of <0.7 μm (≥0.7 μm) (table 1).

The reduced evapotranspiration in response to afforestation means smaller latent heat flux. This, together with the positive change in net radiation, suggests that sensible heat flux would increase (fig. 6). The simulated sensible heat flux and its change show spatial patterns similar to those for net solar radiation, i.e., increase from the western plain to the mountains for the simulation and positive change in the western plain for the response. The magnitude of simulated sensible heat is much smaller, ranging between 10 and 80 W m^{-2}. The magnitude of the response is 30 W m^{-2}. The magnitude of the change during daytime hours is much larger for either sensible or latent heat flux than for net solar radiation (figs. 4b through 4d), suggesting that other mechanisms may play a more important for the changes in sensible and latent heat fluxes than for solar radiation.

Circulation Pattern

The island is located in the far western section of the dominant northwestern Pacific Subtropical High with weak anti-cyclonic (clockwise) airflows. The simulated average ground airflows (fig. 7) are mostly southerly and divided into two major branches when meeting the central range, and the wind speed becomes weaker due to larger friction over land than over the ocean surface. Meanwhile, the sea-land thermal contrast generates sea breezes, which blow toward land (ocean) during day (night) time, as indicated by the positive (negative) sign of zonal wind.

Afforestation leads to remarkable wind speed reduction with both large-scale circulations and local sea breezes in the afforested western plain. The change in the meridional (y) component is negative (northerly wind trend), which is opposite to the simulated southerly wind. The change in the zonal (x) component is negative or easterly (positive or westerly) during day (night) time, opposite to the corresponding simulated westerly (easterly) wind (figs. 4e and 4f).

Responses under Rainy Conditions

To understand the influence of precipitation on ET and

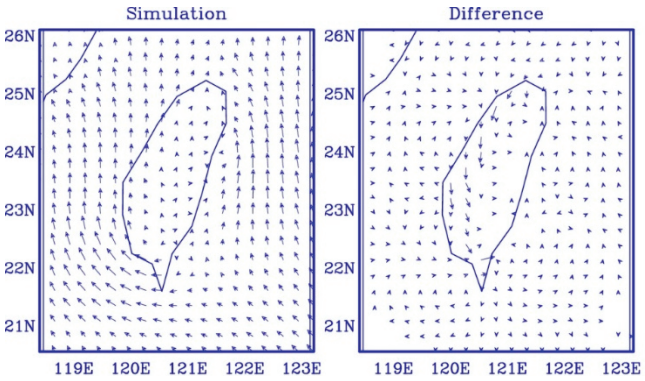

Figure 7. Spatial patterns of wind vectors averaged over the simulation period for the control simulation (left) and the difference between the afforestation and control simulations (right).

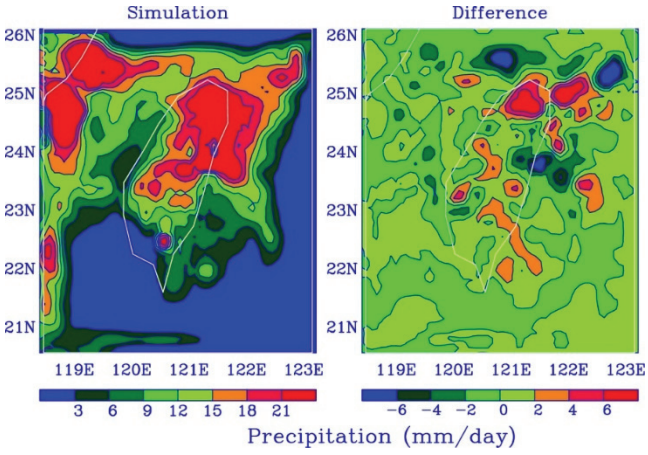

Figure 8. Spatial patterns of precipitation (mm d^{-1}) averaged over the rainy days for the control simulation (left) and the difference between the afforestation and control simulations (right).

heat flux responses, averages were made over the days for the three rainfall events (rainy days) and over other days (clear days). The simulated precipitation averaged over the rainy days appears mainly in northern and central Taiwan (fig. 8). The first major event and the weak event, occurring in the first few days of the simulation period, spread across the entire island except the southwestern and northwestern coastal areas, with rainfall >20 mm d^{-1} in central Taiwan. The second major event, occurring around June 18, spreads across the entire island except the southwest, with rainfall >20 mm d^{-1} only in northern Taiwan (not shown). Precipitation change in response to afforestation appears patchy with alternate positive and negative values across Taiwan; the small magnitudes occur in the western plain, and the large magnitudes occur on the northeastern coast and adjacent ocean area.

The corresponding airflows are mostly easterly east of Taiwan (fig. 9), split into two branches while passing the island, and then merge. The wind response to afforestation is small except in far south, where airflows opposite to the simulated airflows are seen.

The simulated ET averaged over the rainy days has a similar spatial pattern to that averaged over the entire simulation period despite the reduced magnitude in northern Taiwan (fig. 10). However, the response to afforestation is

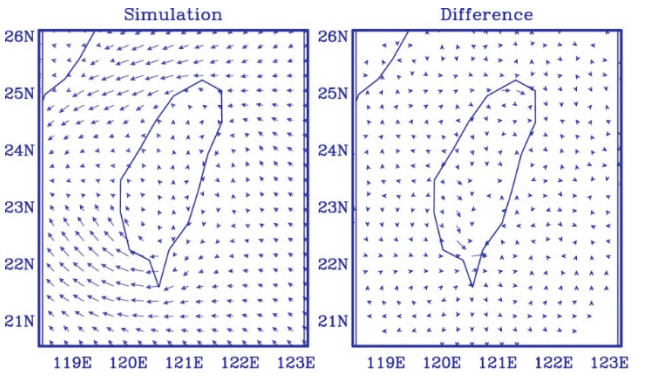

Figure 9. Spatial patterns of wind vectors averaged over the rainy days for the control simulation (left) and the difference between the afforestation and control simulations (right).

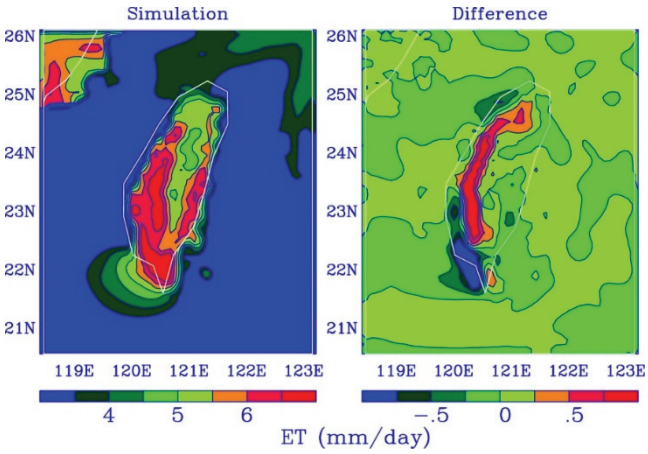

Figure 10. Spatial patterns of ET (mm d^{-1}) averaged over the rainy days for the control simulation (left) and the difference between the afforestation and control simulations (right).

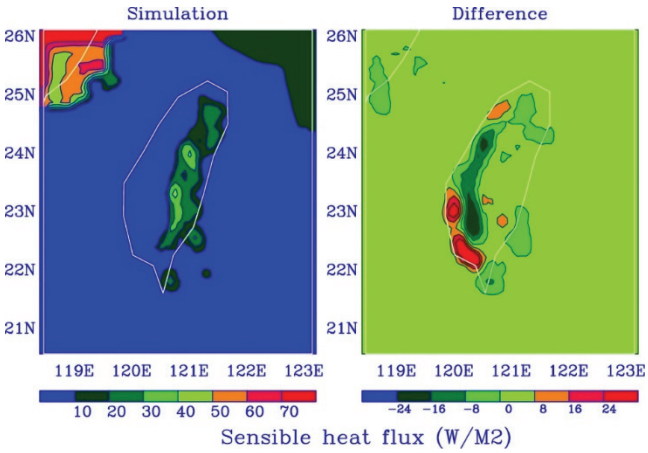

Figure 11. Spatial patterns of sensible heat flux averaged over the rainy days for the control simulation (left) and the difference between the afforestation and control simulations (right).

totally different, as indicated by an overwhelmingly positive change with a magnitude of 0.5 mm d^{-1} in the afforested area except in the far south. The change in sensible heat flux averaged over the rainy days is also opposite to that averaged over the simulation period, with a negative sign in a majority of the afforested area (fig. 11).

The spatial patterns of ET and sensible heat and their

changes averaged over the clear days (not shown) are similar to those averaged over the entire simulation period except with greater magnitude. The changes in ET and sensible heat flux in the spatial distribution are -0.75 mm d^{-1} and 18 W m^{-2}, respectively. The similarity indicates that the change for the clear days contributes more than the change for the rainy days to the overall change for the entire simulation period.

Physical Mechanisms

The large change in L_{SAI} due to afforestation appears to be a major factor for the opposite responses between ET and sensible heat. LAI varies seasonally and is about the same for crops (close to the maximum value of 6.0) and forests (a constant value of 6.0) during June. However, SAI for forests is four times that for crops (table 1). Thus, forests have a much larger L_{SAI} than crops. Sensible heat, which is proportional to L_{SAI} (eq. 2), tends to increase due to afforestation. Evapotranspiration, on the other hand, is proportional to the ratio of LAI to L_{SAI} (eq. 1), which is much smaller for forests than for crops. Thus, latent heat flux and sensible heat flux respond oppositely to afforestation.

For the rainy days, the increase in ET may be caused by the increased water storage capacity on the foliage surface. The intercepted rainfall is proportional to precipitation rate and fractional vegetation cover. In BATS, forests have fractional vegetation cover comparable to that of crops during summer. However, the maximum water content on the foliage surface is proportional to L_{SAI}, which is several times larger than that of crops. This means that much more rain water can be held on the foliage surface and later returned to the air by evaporation. Larger ET from trees consumes more latent heat, and therefore less sensible heat flux is available in forests than in crops.

The changes in other vegetation properties have different impacts on ET and other land surface processes. On one hand, more solar radiation and vegetation lead to larger transpiration. In addition, roughness length is tens of times larger for trees than for crops (table 1). The aerodynamic resistance is therefore much smaller for trees, in favor of increasing water and heat transfer from foliage. On the other hand, afforestation leads to a large decrease in background winds, as shown above. This favors an increase in aerodynamic resistance and therefore decreasing water and heat transfer for forests. The reduced ET due to afforestation implies that the change in background winds should be more important than the changes in solar radiation and roughness.

The changes in temperature and air specific humidity gradients are another mechanism for the responses of ET and sensible heat fluxes to afforestation. However, it is difficult to examine this mechanism because of the complex interactions and feedbacks with the energy fluxes.

Sensitivity Experiments

In comparison with the reference simulation for the dry period, the convection sensitivity experiment produces larger ET, with values exceeding 6 mm d^{-1} in the eastern range and the mainland China coastal area in addition to western Taiwan (fig. 12). In spite of the differences, the changes due to afforestation are the same (i.e., reduced ET in the afforested area) with comparable magnitude among the reference simulation, convection sensitivity experiment, and PBL sensitivity experiment.

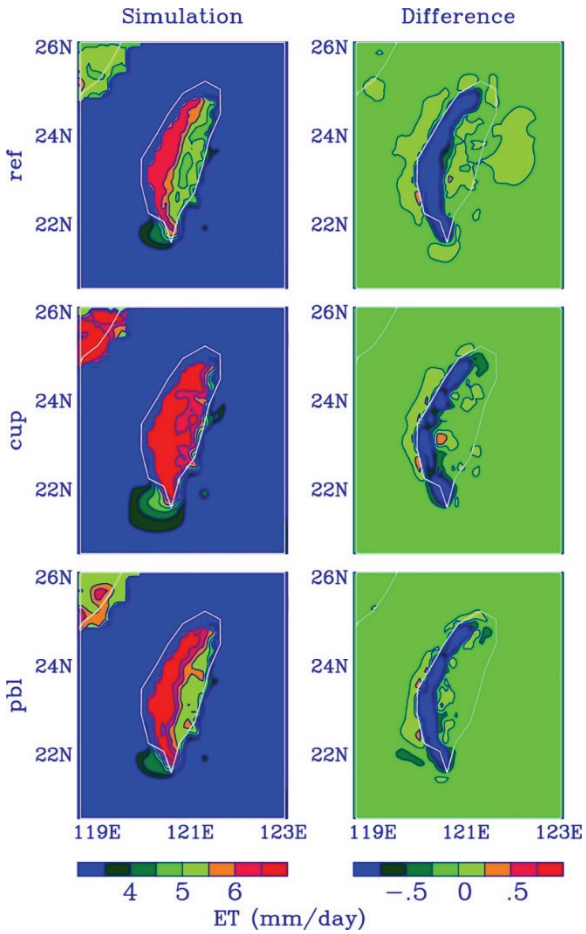

Figure 12. Spatial patterns of ET (mm d^{-1}) averaged over the dry period for the control simulation (left) and the difference between the afforestation and control simulations (right) (ref, cup, and pbl = reference, convection, and PBL sensitivity simulations, respectively).

For the rainy period (fig. 13), differences with the reference simulation are also seen for the convection sensitivity simulation, which has larger ET over the ocean areas south of Taiwan and mainland China. But again, the changes due to afforestation are the same among the reference simulation, convection sensitivity experiment, and PBL sensitivity experiment. The ET changes are positive in most of the afforested region, which is opposite to those for the dry period. Negative values are found in the south and north of the region.

The same responses of ET to afforestation are also seen for other properties, such as radiation, sensible heat flux, temperature, and wind speed (not shown). The results thus indicate that the effects of afforestation simulated with RegCM are robust.

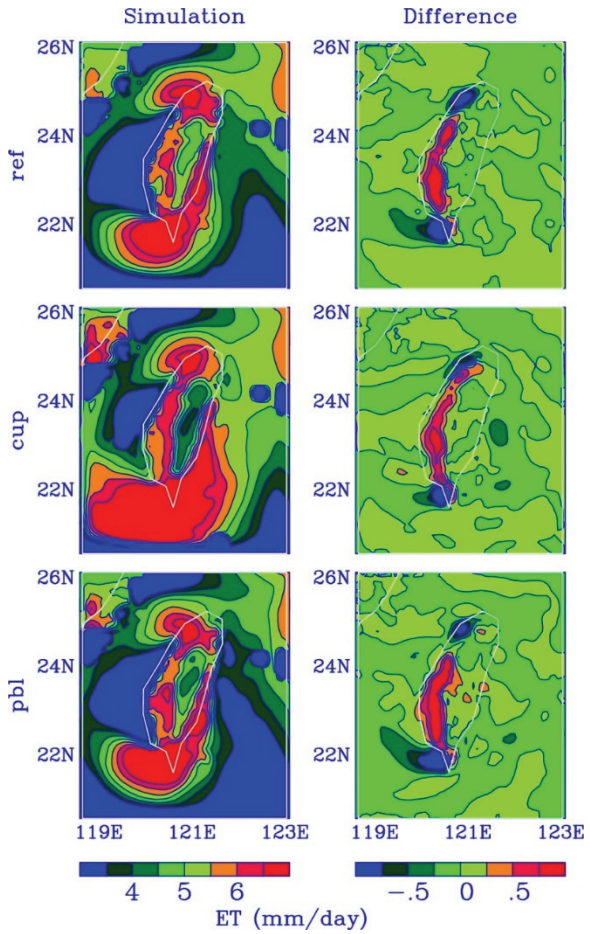

Figure 13. Spatial patterns of ET (mm d^{-1}) averaged over the rainy period for the control simulation (left) and the difference between the afforestation and control simulations (right) (ref, cup, and pbl = reference, convection, and PBL sensitivity simulations, respectively).

DISCUSSION

IMPACTS OF AFFORESTATION

Previous studies on the impacts of land cover change on ET and other land surface processes in other climate regimes show that afforestation generally increases ET and decreases sensible heat flux (Sun and Liu, 2013). One example is the study on the Three-North Shelter Forest Program in northern China (Liu et al., 2008a). The findings from our study for western Taiwan are opposite to the general findings but consistent with those of Liu et al. (2008b), which indicated an increase in annual ET of 182 mm on national average due to cropland expansion in China during the 20th century. The different and even opposite responses to land cover change for ET and sensible heat flux under different climate regimes were noted in a review by Pielke et al. (2011), who stated that, although observational studies from various continents had provided convincing evidence that land cover and land use change plays a significant role in altering surface fluxes, empirical studies are by no means inclusive. There is large variability for the general forest-water relationships, presumably due to the variability of the type, extent, and magnitude of forest disturbances (Sun et al., 2008; Sun and Liu, 2013), climatic regime and distribution (Jones et al., 2012), and ecosystem structure (Ford et al., 2011).

Our study separated rainy days from dry days and found opposite ET changes due to afforestation in Taiwan; ET increased during rainy days but decreased during clear days. Thus, afforestation in this region is likely to modulate extreme hydrological conditions by evaporating less (more) water during clear (rainy) periods and reduce the risks of droughts and floods to a certain extent. Climate and hydrological extremes and their future trends have become an important issue owing to the rise in water demand and looming climate change (Mishra and Singh, 2010). The findings from our study suggest the potential role of afforestation in mitigating the impacts of extreme conditions.

LAND SURFACE MODELING

The complexity in the afforestation responses may be also related to the assumptions used by various models to simulate ET and energy balance. As described above, sensible heat flux (ET) is proportional (inversely proportional) to L_{SAI} in BATS. Afforestation in the western plain of Taiwan increases L_{SAI} and therefore leads to increased (decreased) sensible (latent) heat flux. In some other models, such as the Simple Biosphere Model (SiB) (Sellers et al., 1986), the roles of the vegetation area indexes, which are considered in calculating the bulk boundary layer resistance of the leaf surface and stomatal resistance, are the same for sensible heat flux and evaporation. Thus, smaller difference in the responses between the two types of fluxes would be expected from SiB. The land surface scheme is critical to this study. There have been improvements to BATS, and new schemes such as Community Land Model (CLM) (Oleson et al., 2010) are now available in RegCM. Applications of these improved schemes should improve this study.

PHYSICAL FACTORS

Albedo, stem area index, and roughness are important factors for the impacts of afforestation on ET and other land surface processes. A possible approach to fully understand the relative importance of the three factors is to conduct sensitivity experiments to examine how much the responses of ET and other land surface processes to afforestation vary with each factor. Although such experiments were not conducted in this study, the relative importance of the three factors can be expected through the following two-step comparisons. The first step is to find the most important factor. The change in either albedo or roughness due to afforestation would have similar impacts on ET and sensible heat flux. Reduced albedo would provide more energy to the water and heat fluxes, while increased roughness would reduce wind speed and the water and heat fluxes. However, the change in stem area index would lead to opposite changes in ET and sensible heat flux, and to opposite changes in ET between dry and rainy periods. Thus, we could first assume that the modeling results would be most sensitive to stem area index among the three factors. The second step is to find the second important factor. The land change from crops to forests would lead to larger change in

roughness than albedo due to the big difference in the plant height and the small difference in plant color. Thus, we could further assume that the modeling results would be more sensitive to roughness than albedo between the two factors.

Another important issue that was not analyzed in this study is the possible impact of the changes in soil properties due to afforestation. Afforestation would change soil properties (porosity, hydraulic conductivity, tension at saturation, wetness parameters, etc.), which would in turn affect ET and other land surface processes. Kim et al. (2005) showed the differences in these properties between paddy field and forests in Thailand and examined the ET impacts of these properties together with the differential properties in vegetation and physiology.

MODEL DYNAMICS

Our simulations used 14 vertical atmosphere layers, with only five of them in the PBL. This could impact our simulations in several ways. First, all land surface fluxes calculated with BATS need atmospheric conditions of temperature, humidity, and wind speed right above the ground. They were obtained from the lowest atmospheric level in RegCM. Fewer model layers in the PBL means a greater distance from that level to the ground, which leads to larger bias in determining the air conditions on the ground. Secondly, PBL height is an important parameter for the development of turbulence and eddies. For the same reason, fewer model layers in the PBL would lead to larger bias in calculating this parameter. Thirdly, the PBL usually includes the surface layer and mixed layer, which have different properties with turbulent fluxes. Fewer model layers would increase the difficulty in accurately determining the interface of the two layers. In future modeling studies, higher vertical resolution in the PBL should be used to reduce the related biases.

A simulation with an RCM often uses a spin-up time to make the various components in a soil-atmosphere-vegetation system adjust to each other. Such a spin-up process was not included in this study. Second, the monsoon climate has large inter-annual variability. Thus, simulation of a specific year is only considered a case study. Fixed ocean condition is a common approach for most regional climate modeling. For simulation of the Taiwan island, however, sea breeze is an important local process for precipitation and temperature in the western plain, while changes in the thermal condition of the ocean may affect the development of sea breezes and the responses to afforestation investigated in this study. This possible impact needs to be examined.

As described in the Method section, the hydrostatic assumption is a major limitation of this study. Non-hydrostatic dynamics have been adopted in RegCM to predict vertical motion. Applications of the new RegCM as well as other non-hydrostatic models such as the Weather Research and Forecast (WRF) model (Skamarock et al., 2008) and the Advanced Regional Prediction System (ARPS) (Xue et al., 2000, 2001) with increased grid resolution should improve the simulation of afforestation effects in Taiwan by more realistically describing the atmospheric processes in the central range.

CONCLUSIONS

Numerical simulations and sensitivity experiments were performed using RegCM to investigate the impacts of land cover conversion from crops to forests in western Taiwan on ET and other land surface processes. The results indicated that afforestation may have different ET changes depending on weather conditions. ET would decrease during clear days due to afforestation but increase during rainy days. Thus, afforestation in this region is likely to modulate extreme hydrological conditions by evaporating less (more) water during clear (rainy) periods and reduce the risks of droughts and floods to a certain extent. However, the results may be influenced by many model limitations, including applications of the hydrostatic assumption and the low vertical resolution of the model. The responses of soil properties to afforestation were not investigated in this study. Future studies should be conducted for longer periods with model parameters derived locally.

ACKNOWLEDGEMENTS

The authors would like to thank the four reviewers for their constructive comments and the Associate Editor for insightful and detailed suggestions that greatly improved the manuscript. This research was supported by the USDA Forest Service.

REFERENCES

Anthes, R. A. (1977). A cumulus parameterization scheme utilizing a one-dimensional cloud model. *Monthly Weather Rev., 105*(3), 270-286. http://dx.doi.org/10.1175/1520-0493(1977)105<0270:ACPSUA>2.0.CO;2.

Anthes, R. A., Hsie, E.-Y., & Kuo, Y.-H. (1987). Description of the Penn State/NCAR Mesoscale Model Version 4 (MM4). Technical Note NCAR/TN-282+STR. Boulder, Colo.: National Center for Atmospheric Research.

Arakawa, A., & Schubert, W. H. (1974). Interaction of a cumulus cloud ensemble with the large-scale environment: Part I. *J. Atmos. Sci., 31*(3), 674-701. http://dx.doi.org/10.1175/1520-0469(1974)031<0674:IOACCE>2.0.CO;2.

Briegleb, B. P. (1992). Delta-Eddington approximation for solar radiation in the near community climate model. *J. Geophys. Res., 97*(D7), 7603-7612. http://dx.doi.org/10.1029/92JD00291.

Dickinson, R. E., Errico, R. M., Giorgi, F., & Bates, G. T. (1989). A regional climate model for the western U.S. *J. Climate, 15*(3), 383-422.

Dickinson, R. E., Henderson-Sellers, A., Kennedy, P. J., & Giorgi, F. (1993). Biosphere-Atmosphere Transfer Scheme (BATS) Version 1e as coupled to the NCAR Community Climate Model. Technical Note NCAR/TN-387+STR. Boulder, Colo.: National Center for Atmospheric Research.

Elguindi, N., Bi, X., Giorgi, F., Nagarajan, B., Pal, J., Solmon, F., Rauscher, S., & Zakey, A. (2007). *RegCM Version 3.1 User's Guide*. Trieste, Italy: International Center for Theoretical Physics (ICTP).

Fang, J., Chen, A., Peng, C., Zhao, S., & Ci, L. (2001). Changes in forest biomass carbon storage in China between 1949 and 1998.

Science, 292(5525), 2320-2322. http://dx.doi.org/10.1126/science.1058629.
Ford, C. R., Laseter, S. H., Swank, W. T., & Vose, J. M. (2011). Can forest management be used to sustain waterbased ecosystem services in the face of climate change? *Ecol. Appl., 21*(6), 2049-2067. http://dx.doi.org/10.1890/10-2246.1.
Giorgi, F., & Bates, G. T. (1989). The climatological skill of a regional model over complex terrain. *Monthly Weather Rev., 117*(11), 2325-2347. http://dx.doi.org/10.1175/1520-0493(1989)117<2325:TCSOAR>2.0.CO;2.
Giorgi, F., Marinucci, M. R., De Canio, G., & Bates, G. T. (1993a). Development of a second-generation regional climate model (RegCM2): I. Boundary layer and radiative transfer processes. *Monthly Weather Rev., 121*(10), 2794-2813. http://dx.doi.org/10.1175/1520-0493(1993)121<2794:DOASGR>2.0.CO;2.
Giorgi, F., Marinucci, M. R., De Canio, G., & & Bates, G. T. (1993b). Development of a second-generation regional climate model (RegCM2): II. Convective processes and assimilation of lateral boundary conditions. *Monthly Weather Rev., 121*(10), 2814-2832. http://dx.doi.org/10.1175/1520-0493(1993)121<2814:DOASGR>2.0.CO;2.
Giorgi, F., & Shields, C. (1999). Tests of precipitation parameterizations available in latest version of NCAR regional climate model (RegCM) over continental U.S. *J. Geophys. Res., 104*(D6), 6353-6375. http://dx.doi.org/10.1029/98JD01164.
Grell, A. G. (1993). Prognostic evaluation of assumptions used by cumulus parameterizations. *Monthly Weather Rev., 121*(3), 764-787. http://dx.doi.org/10.1175/1520-0493(1993)121<0764:PEOAUB>2.0.CO;2.
Holtslag, A. A. M., & Boville, B. A. (1993). Local versus nonlocal boundary-layer diffusion in a global climate model. *J. Climate, 6*(10), 1825-1842. http://dx.doi.org/10.1175/1520-0442(1993)006<1825:LVNBLD>2.0.CO;2.
Holtslag, A. A. M., De Bruijn, E. I. F., & Pan, H.-L. (1990). A high-resolution air mass transformation model for short-range weather forecasting. *Monthly Weather Rev., 118*(8), 1561-1575. http://dx.doi.org/10.1175/1520-0493(1990)118<1561:AHRAMT>2.0.CO;2.
Jackson, R., Jobbagy, B. E. G., Avissar, R., Roy, S. B., Barrett, D. J., Cook, C. W., ... Murray, B. C. (2005). Trading water for carbon with biological carbon sequestration. *Science, 310*(5756), 1944-1947. http://dx.doi.org/10.1126/science.1119282.
Jones, J. A., Creed, I. F., Hatcher, K. L., Warren, R. J., Adams, M. B., Benson, M. H., ...Williams, M. W. (2012). Ecosystem processes and human influences regulate streamflow response to climate change at long-term ecological research sites. *BioSci., 62*(4), 390-404. http://dx.doi.org/10.1525/bio.2012.62.4.10.
Kato, H., Hirakuchi, H., Nishizawa, K., & Giorgi, F. (1999). Performance of NCAR RegCM in the simulation of June and January climates over eastern Asia and the high-resolution effect of the model. *J. Geophys. Res., 104*(D6), 6455-6476. http://dx.doi.org/10.1029/1998JD200041.
Kiehl, J. T., Hack, J. J., Bonan, G. B., Boville, B. A., Breigleb, B. P., Williamson, D. L., & Rasch, P. J. (1996). Description of the NCAR Community Climate Model (CCM3). Technical Note NCAR/TN-420+STR. Boulder, Colo.: National Center for Atmospheric Research.
Kim, W., Kanae, S., Agata, Y., & Oki, T. (2005). Simulation of potential impacts of land use//cover changes on surface water fluxes in the Chaophraya river basin, Thailand. *J. Geophys. Res., 110*(D8), D08110. http://dx.doi.org/10.1029/2004JD004825.
Kuo, H.-L. (1974). Further studies of the parameterization of the influence of cumulus convection on large-scale flow. *J. Atmos. Sci., 31*(5), 1232-1240. http://dx.doi.org/10.1175/1520-0469(1974)031<1232:FSOTPO>2.0.CO;2.
Li, Y., Zhao, M., Motesharrei, S., Mu, Q., Kalnay, E., & Li, S. (2015). Local cooling and warming effects of forests based on satellite observations. *Nature Communications, 6*, article 6603.
Lin, C. Y., Chen, W. C., Liu, S. C., Liou, Y. A., Liu, G. R., & Lin, T. H. (2008). Numerical study of the impact of urbanization on the precipitation over Taiwan. *Atmos. Environ., 42*(13), 2934-2947. http://dx.doi.org/10.1016/j.atmosenv.2007.12.054.
Liu, M. L., Tian, H. Q., Chen, G. S., Wei, R., Zhang, C., & Liu, J. Y. (2008a). Effects of land use and land-cover change on evapotranspiration and water yield in China during 1900-2000. *JAWRA, 44*(5), 1193-1207. http://dx.doi.org/10.1111/j.1752-1688.2008.00243.x.
Liu, T.-J. (1998). Han migration and the settlement of Taiwan: The onset of environmental change. In M. Elvin and L. Ts'ui-jung (eds), *Sediment of Time: Environment and Society in Chinese History* (pp. 165-199). New York, N.Y.: Cambridge University Press.
Liu, Y. Q., Avissar, R., & Giorgi, F. (1996). Simulation with the regional climate model RegCM2 of extremely anomalous precipitation during the 1991 east Asian flood: An evaluation study. *J. Geophys. Res., 101*(D21), 26199-26215. http://dx.doi.org/10.1029/96JD01612.
Liu, Y. Q., Giorgi, F., & Washington, W. M. (1994). Simulation of summer monsoon climate over east Asia with an NCAR regional climate model. *Monthly Weather Rev., 122*(10), 2331-2348. http://dx.doi.org/10.1175/1520-0493(1994)122<2331:SOSMCO>2.0.CO;2.
Liu, Y. Q., Stanturf, J., & Lu, H. (2008b). Modeling the potential of the northern China forest shelterbelt in improving hydroclimate conditions. *JAWRA, 44*(5), 1176-1192. http://dx.doi.org/10.1111/j.1752-1688.2008.00240.x.
McVicar, T. R., Li, L. T., Niel, T. G. V., Zhang, L., Li, R., Yang, Q. K., ... Gao, P. (2007). Developing a decision support tool for China's re-vegetation program: Simulating regional impacts of afforestation on average annual streamflow in the Loess Plateau. *Forest Ecol. Mgmt., 251*(1-2), 65-81. http://dx.doi.org/10.1016/j.foreco.2007.06.025.
Mishra, A. K., & Singh, V. P. (2010). A review of drought concepts. *J. Hydrol., 391*(1-2), 202-216. http://dx.doi.org/10.1016/j.jhydrol.2010.07.012
Misra, V., & Dirmeyer, P. A. (2009). Air, sea, and land interactions of the continental U.S. hydroclimate. *J. Hydrometeorol., 10*(2), 353-373. http://dx.doi.org/10.1175/2008JHM1003.1.
Oleson, K. W., Lawrence, D. M., Bonan, G. B., Flanner, M. G., Kluzek, E., Lawrence, P. J., ... Zeng, X. (2010). Technical description of Version 4.0 of the Community Land Model (CLM). NCAR Technical Note NCAR/TN-478+STR. Boulder, Colo.: National Center for Atmospheric Research.
Pielke, R. A., Pitman, A., Niyogi, D., Mahmood, R., McAlpine, C., Hossain, F., ... de Noblet, N. (2011). Land use/land cover changes and climate: Modeling analysis and observational evidence. *WIREs Climate Change, 2*(6), 828-850. http://dx.doi.org/10.1002/wcc.144.
Sampson, R. N. (2004). Southern forests: Yesterday, today, and tomorrow. In H. M. Rauscher, & K. Johnson (Eds.), *Southern Forest Science: Past, Present, and Future* (pp. 5-14). General Technical Report SRS-75. Asheville, N.C.: USDA Forest Service Southern Research Station.
Schleeter, R. (2013). The Great Green Wall: Sahel-Sahara project aims to combat land degradation. Washington, D.C.: National Geographic Society. Retrieved from http://education.nationalgeographic.com.au/education/news/great-green-wall/?ar_a=1#page=1.
Sellers, P. J., Mintz, Y., Sud, Y. C., & Dalcher, A. (1986). A simple

biosphere model (SiB) for use within general circulation models. *J. Atmos. Sci., 43*(6), 505-531. http://dx.doi.org/10.1175/1520-0469(1986)043<0505:ASBMFU>2.0.CO;2.

Seth, A., & Giorgi, F. (1998). The effects of domain choice on summer precipitation simulation and sensitivity in a regional climate model. *J. Climate, 11*(10), 2698-2712. http://dx.doi.org/10.1175/1520-0442(1998)011<2698:TEODCO>2.0.CO;2.

Shea, D. J., Trenberth, K. E., & Reynolds, R. W. (1992). A global monthly sea surface temperature climatology. *J. Climate, 5*(9), 987-1001. http://dx.doi.org/10.1175/1520-0442(1992)005<0987:AGMSST>2.0.CO;2.

Shen, S. S. (2009). Mitigating climate change: What Taiwan is doing. Taipei, Taiwan: Environmental Protection Administration. Retrieved from http://unfccc.epa.gov.tw/unfccc/english/_uploads/downloads/03_Mitigating_Climate_Change-What_Taiwan_is_Doing.pdf.

Skamarock, W. C., Klemp, J. B., Dudhia, J., Gill, D. O., Barker, D. M., Duda, M. G., ... Powers, J. G. (2008). A description of the advanced research WRF Version 3. Technical Note NCAR/TN-475+STR. Boulder, Colo.: National Center for Atmospheric Research.

Slingo, A. (1989). A GCM parameterization for the shortwave radiative properties of water clouds. *J. Atmos. Sci., 46*(10), 1419-1427.

Sun, G., & Liu, Y. Q. (2013). Forest influences on climate and water resources at the landscape to regional scale. In B. Fu, & B. Jones (Eds.), *Landscape Ecology for Sustainable Environment and Culture* (pp. 309-334). New York, N.Y.: Springer. http://dx.doi.org/10.1007/978-94-007-6530-6_15.

Sun, G., Zuo, C. Q., Liu, S. Y., Liu, M. L., McNulty, S. G., & Vose, J. M. (2008). Watershed evapotranspiration increased due to changes in vegetation composition and structure under a subtropical climate. *JAWRA, 44*(5), 1164-1175. http://dx.doi.org/10.1111/j.1752-1688.2008.00241.x.

Trenberth, K. E., & Olson, J. G. (1988). ECMWF Global Analyses 1979-1986: Circulation statistics and data evaluation. Technical Note NCAR/TN-300+ STR. Boulder, Colo.: National Center for Atmospheric Research.

USDA Forest Service. (1994). Pest and pesticide management on southern forests. Management Bull. R8-MB 60. Atlanta, Ga.: USDA Forest Service.

Wu, R.-S., Sue, W.-R., Chien, C.-B., Chen, C.-H., Chang, J.-S., & Lin, K.-M. (2001). A simulation model for investigating the effects of rice paddy fields on the runoff system. *Math. Comput. Model., 33*(6-7), 649-658. http://dx.doi.org/10.1016/S0895-7177(00)00269-7.

Xue, M., Droegemeier, K. K., & Wong, V. (2000). The Advanced Regional Prediction System (ARPS): A multiscale nonhydrostatic atmospheric simulation and prediction tool: Part I. Model dynamics and verification. *Meteorol. Atmos. Phys., 75*(3), 161-193. http://dx.doi.org/10.1007/s007030070003.

Xue, M., Droegemeier, K., Wong, V., Shapiro, A., Brewster, K., Carr, F., ... Wang, D.-H. (2001). The Advanced Regional Prediction System (ARPS): A multiscale nonhydrostatic atmospheric simulation and prediction tool: Part II. Model physics and applications. *Meteorol. Atmos. Phys., 76*(3), 143-165. http://dx.doi.org/10.1007/s007030170027.

Zeng, X., Dickinson, R. E., Walker, A., Shaikh, M., DeFries, R. S., & & Qi, J. (2000). Derivation and evaluation of global 1-km fractional vegetation cover data for land modeling. *J. Appl. Meteorol., 39*(6), 826-839. http://dx.doi.org/10.1175/1520-0450(2000)039<0826:DAEOGK>2.0.CO;2.

Zhan, X. S., Zhao, J., Wang, H. X., & Yin, J. (2011). Quantitative estimation of land surface evapotranspiration in Taiwan based on MODIS data. *Water Sci. Eng., 4*(3), 237-245. http://dx.doi.org/doi:10.3882/j.issn.1674-2370.2011.03.001.

Zhang, K., Yu, Z., Li, X., Zhou, W., & Zhang, D. (2007). Land use change and land degradation in China from 1991 to 2001. *Land Degrad. Devel., 18*(2), 209-219. http://dx.doi.org/10.1002/ldr.757.